Explosion mechanisms at Arenal volcano, Costa Rica: An interpretation from integration of seismic and Doppler radar data

S. Valade,[1,2,3] F. Donnadieu,[1,2,3] P. Lesage,[4] M. M. Mora,[5] A. Harris,[1,2,3] and G. E. Alvarado[5]

Received 23 June 2011; revised 15 November 2011; accepted 17 November 2011; published 21 January 2012.

[1] We execute an integrated analysis of broadband seismic and Doppler radar data to gain insights into the subsurface mechanisms that drive repetitive, mildly explosive activity of Arenal volcano (Costa Rica). We find large variability of both seismic and radar waveforms, and nonsystematic relationships between the two. Seismic recordings display long-lasting tremor sequences and numerous explosion quakes. Radar measurements show that tephra emissions are poorly correlated, in both time and energy, to the seismic activity. Tephra emissions were found in association with explosion quakes but also during episodes of tremor and seismic quiescence. Moreover, the exit velocity, mass loading, and kinetic energy of the emissions show no clear relationship with the coeval seismic amplitude and frequency content. We propose a conceptual source model whereby degasing is controlled by opening and closing of fractures that crosscut a rigid cap atop the conduit. When the fracture's strength is overcome by the gas pressure building up below, it suddenly opens and high-velocity gas escapes, producing high-frequency elastic waves typical of explosion quakes. Gas release also occurs in relation to periodic opening and closure of the fractures to produce repetitive pressure pulses, this being the source of tremor. In both cases, varying quantities of fragmented material may be carried by the gas, which can be detected by the radar if their concentration is high enough. Moreover, the highly variable, constantly changing state of lava cap (e.g., thickness, fracture network and gas permeability) results in nonrepeatable source conditions and explains the complex relationship between tephra emissions and associated seismic signals.

Citation: Valade, S., F. Donnadieu, P. Lesage, M. M. Mora, A. Harris, and G. E. Alvarado (2012), Explosion mechanisms at Arenal volcano, Costa Rica: An interpretation from integration of seismic and Doppler radar data, *J. Geophys. Res.*, *117*, B01309, doi:10.1029/2011JB008623.

1. Introduction

[2] Arenal, a small stratovolcano (1,710 m asl) located in northern Costa Rica, has experienced near continuous effusive and explosive activity since its reactivation in 1968 [*Minakami et al.*, 1969; *Cigolini and Borgia*, 1980]. Since 1975, the activity has been concentrated in crater C, from which blocky basaltic-andesitic lavas continuously effuse [*Cigolini et al.*, 1984; *Murillo and Ruiz*, 2004]. In addition, pyroclastic flows and numerous small ash plumes (ascending ≤1–3 km above the crater) are emitted recurrently [*Cole et al.*, 2005]. The frequency of ash emissions in the 1980s and 1990s was nearly one event every 30 min [*Williams-Jones et al.*, 2001], but this frequency has been progressively decreasing so that only a few per day were recorded during the time of our recording campaign in 2005. Arenal's lava discharge rate also fell from ~2 m^3/s in the 1980s to between 0.1 and 0.2 m^3/s in 2004 [*Wadge et al.*, 2006], and a rigid degassed plug capping the conduit has developed [*Cole et al.*, 2005].

[3] A number of geophysical studies have been carried at Arenal in order to constrain its shallow structure and the mechanisms operating within it. Studies using seismic data have constrained the shallow velocity structure of the edifice [*Mora et al.*, 2006], as well as the source mechanism of both tremor [*Benoit and McNutt*, 1997; *Lesage et al.*, 2006] and long period signals [*Davi et al.*, 2010]. *Hagerty et al.* [2000]

[1]Clermont Université, Université Blaise Pascal, Observatoire de Physique du Globe de Clermont-Ferrand, Laboratoire Magmas et Volcans, Clermont-Ferrand, France.
[2]Also at CNRS, UMR 6524, Laboratoire Magmas et Volcans, Clermont-Ferrand, France.
[3]Also at Institut de Recherche pour le Développement, R 163, Laboratoire Magmas et Volcans, Clermont-Ferrand, France.
[4]Institut des Sciences de la Terre, Université de Savoie, CNRS, Le Bourget-du-Lac, France.
[5]Escuela Centroamericana de Geología, Universidad de Costa Rica, San José, Costa Rica.

0148-0227/12/2011JB008623

cross-correlated seismic and acoustic data, and achieved a detailed analysis of the waveforms to give further constraints on the generation of these signals. *Williams-Jones et al.* [2001] cross-correlated seismic data with both SO_2 fluxes (from COSPEC data) and Earth tides to investigate the link between degassing, seismicity, and the influence of cyclic drivers. No study, however, has been able to cross-correlate quantitative information regarding both the pyroclastic emissions and subsurface processes that drive the explosions.

[4] We here quantify the exit velocity, mass-loading and kinetic energy proxies of pyroclastic emissions using ground-based Doppler radar (VOLDORAD), which we cross-correlate with broadband seismic data. We use these data to constrain a conceptual model which accounts for the complex interplay between tremor, explosion earthquakes and tephra emissions recorded in this study.

2. Background: Seismic Activity at Arenal

[5] Arenal exhibits intense and varied seismic activity, including tremor, explosion quakes, long-period (LP) events, rockfall events, and (rarer) volcano-tectonic events. Tremor is the most common signal, it being recorded several hours per day on average. Two types of tremor are commonly distinguished depending on the way the energy is distributed across the spectrum [*McNutt*, 2002]: when the energy is evenly distributed with no dominant peak (generally confined to the 1–6 Hz band at Arenal), it is referred to as "spasmodic tremor"; if the spectrum contains several regularly spaced peaks, composed of a fundamental frequency and its overtones, it is termed "harmonic tremor." The fundamental frequency at Arenal is generally in the range 0.9–2 Hz [*Hagerty et al.*, 2000; *Mora*, 2003], and the frequencies of overtones are integer multiples of it. Tremor at Arenal shows striking characteristics, such as [*Lesage et al.*, 2006]: frequency gliding episodes (whereby the fundamental and corresponding harmonic frequencies fluctuate in time while maintaining their regular spacing [*Benoit and McNutt*, 1997; *Garcés et al.*, 1998; *Hagerty et al.*, 2000]), frequency jumps (with either positive or negative increments), progressive transitions from spasmodic to harmonic tremor (with variable quantities of harmonic overtones), and coexistence of multiple frequency systems (with distinct spectral peaks and independent gliding). Several source models have been proposed to explain tremor at many volcanoes worldwide; at Arenal the clarinet model defined by *Lesage et al.* [2006] appears to be well-adapted to describe the complex behavior of the tremor. In particular, harmonic and spasmodic tremor are thought to have the same source mechanism, i.e., intermittent flow of gas through fractures in the cap atop the conduit. Frequency gliding is attributed to pressure fluctuations in the magmatic conduits [*Neuberg*, 2000; *Lesage et al.*, 2006], which depends on the mechanical state of the plug, and also potentially affects its permeability to gas flow. The coexistence of different frequency systems, each evolving independently, may be the expression of different resonators, i.e., different conduits in the shallow feeding system.

[6] Long-period (LP) transients and explosion quakes are regularly superimposed on the nearly continuous tremor, and are both characterized by spindle-shaped envelopes and narrow band-width (1–3 Hz) frequencies [*Chouet*, 1996; *Hagerty et al.*, 2000]. The coda may in some cases evolve into harmonic tremor [*Barquero et al.*, 1992; *Benoit and McNutt*, 1997; *Hagerty et al.*, 2000]. Both LP and explosion quake signals are thought to have the same source mechanism, but with differing source depths. Following *Mori et al.* [1989], explosion quakes should occur at shallow levels within the conduit, allowing the propagation of an acoustic air wave which couples with the ground as a high frequency seismic phase and arrives shortly after the P wave onset. LP events, on the other hand, should occur at greater depths in the conduit, preventing the propagation of an acoustic air wave. Because there is probably no fundamental difference in their mechanisms, we follow *Lesage et al.* [2006] and consider both LP events and explosion quakes as part of the same type of event, defined as "explosion quakes." Note that this term will refer to this particular seismic signal, regardless of whether it is accompanied by tephra emission or not. On the contrary, the term "eruptive event" will refer to tephra emission, regardless of the presence and type of associated seismic signal.

[7] High frequency events are also frequently observed and show a progressive onset followed by a progressive decay, generally lasting 50–180 s. Energy is well staggered between 5 and 35 Hz with no dominant frequency and a sharp onset in the 5–15 Hz band. At Arenal, radar signals are always recorded ahead of these seismic signals. *Johnson and Lees* [2000] described similar events at Karymsky volcano, and suggested that they may result from energetic gas jetting when the vent is unobstructed by debris.

[8] Volcano-tectonic events are less frequent at Arenal as the open state of the vent prevents the accumulation of high stresses. The rarity of such events also suggests the absence of a shallow magma storage body [*Mora*, 2003].

3. Data Acquisition and Processing

[9] VOLDORAD 2 (Volcano Doppler Radar) is a ground-based, pulsed, Doppler radar specifically designed for active remote sensing of volcanic pyroclastic emissions [*Dubosclard et al.*, 1999, 2004; *Donnadieu et al.*, 2003, 2005, 2011; *Gouhier and Donnadieu*, 2008, 2010; *Valade and Donnadieu*, 2011]. It was set up at an altitude of about 690 m asl, around 2.3 km west, and downwind, of active crater C (Figure 1a), from where we recorded activity for several hours per day between February 10 and 22, 2005. The antenna pointed along an azimuth toward the crater, and then lowered until ground echoes appeared in the Doppler spectra, indicating that the base of the beam was aligned with Arenal's summit. At Arenal, there is no deep crater, but rather an irregular dome-like surface. This ensures that the beam skims the eruptive vent. The radar should thus capture all ash emissions, provided the particle concentration is above the detection threshold (ca. 15 g/m^3 for 1 mm particles, *Donnadieu et al.* [2011]). The radar beam is divided into successive sampling volumes, termed range gates, whose radial resolution depend on the pulse duration (τ), and whose location and azimuthal resolution depend on the beam aperture (conical 9° beam width) and the distance from the radar. During the recording campaign, data were recorded in range gates with radial resolutions of 120 m (τ = 0.8 μs), and with slant distances ranging

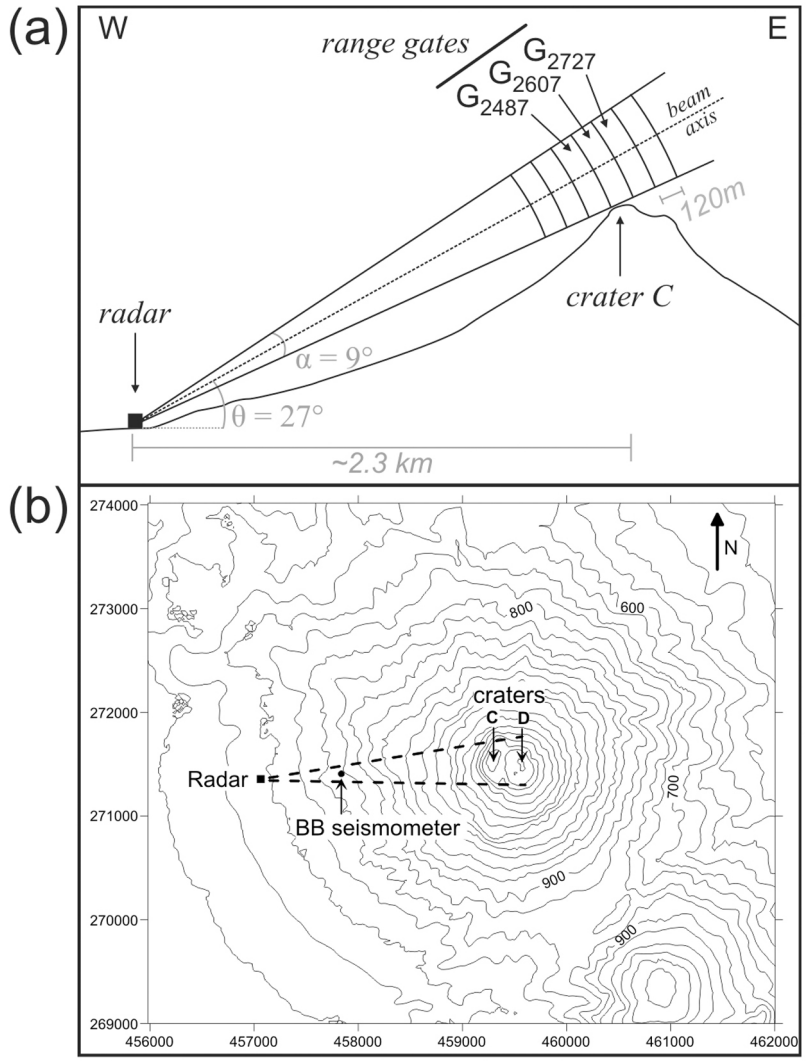

Figure 1. (a) Radar beam geometry during the recording campaign. (b) Location map of the broadband seismometer and Doppler radar. At the time of the recording campaign in February 2005, the estimated altitude of crater C is 1710 m above sea level (asl) [*Wadge et al.*, 2006].

between 2007 and 2847 m (i.e., between gates G_{2007} and G_{2847}). Two range gates were located above the active crater area: gates G_{2607} and G_{2727} (Figure 1a). Volcanic ejecta crossing the beam scatter the electromagnetic signal repeatedly transmitted by the radar (sampling rate 100 μs^{-1}), part of which is scattered back to the radar and can be recorded. Real-time processing of this signal gives information on (1) the backscattered power (which is a complex function of the number and size of the ejecta, and so is a proxy for the mass loading of the pyroclastic emissions), and (2) the radial velocity of the ejecta (i.e., the component of the exit velocity projected along the beam axis). These data are displayed for each range gate as Doppler spectra, representing the backscattered power (P in dB) versus the radial velocity (V in m/s). Processing of the Doppler spectra gives, for each range gate, two sets of parameters: positive parameters, which refer to signal backscattered by particles with a radial component of motion away from the radar, and negative parameters, which refer to particles with a radial motion toward the radar.

[10] For each range gate, the following parameters were defined and calculated: backscattered powers (P_+, P_-, and $P = P_+ + P_-$), and maxima of radial velocities (V_{+max}, V_{-max}) [*Dubosclard et al.*, 2004]. We also implemented a proxy for the kinetic energy E_k of the tephra emission following:

$$E_k = \int_{V-\max}^{V+\max} \left(P(V) \cdot V^2\right).dV \qquad (1)$$

in which V is the radial velocity of particles and P(V) is the power backscattered by all particles with radial velocity V.

[11] Seismic observations were carried out 1.8 km west of the active crater using a permanent 30-s GURALP CMG-6TD broadband seismometer (Figure 1b). The vertical component was generally used, because tremor and explosion quakes are mainly composed of Rayleigh waves [*Mora et al.*, 2006, *Zobin et al.*, 2009], which are polarized in the vertical plane.

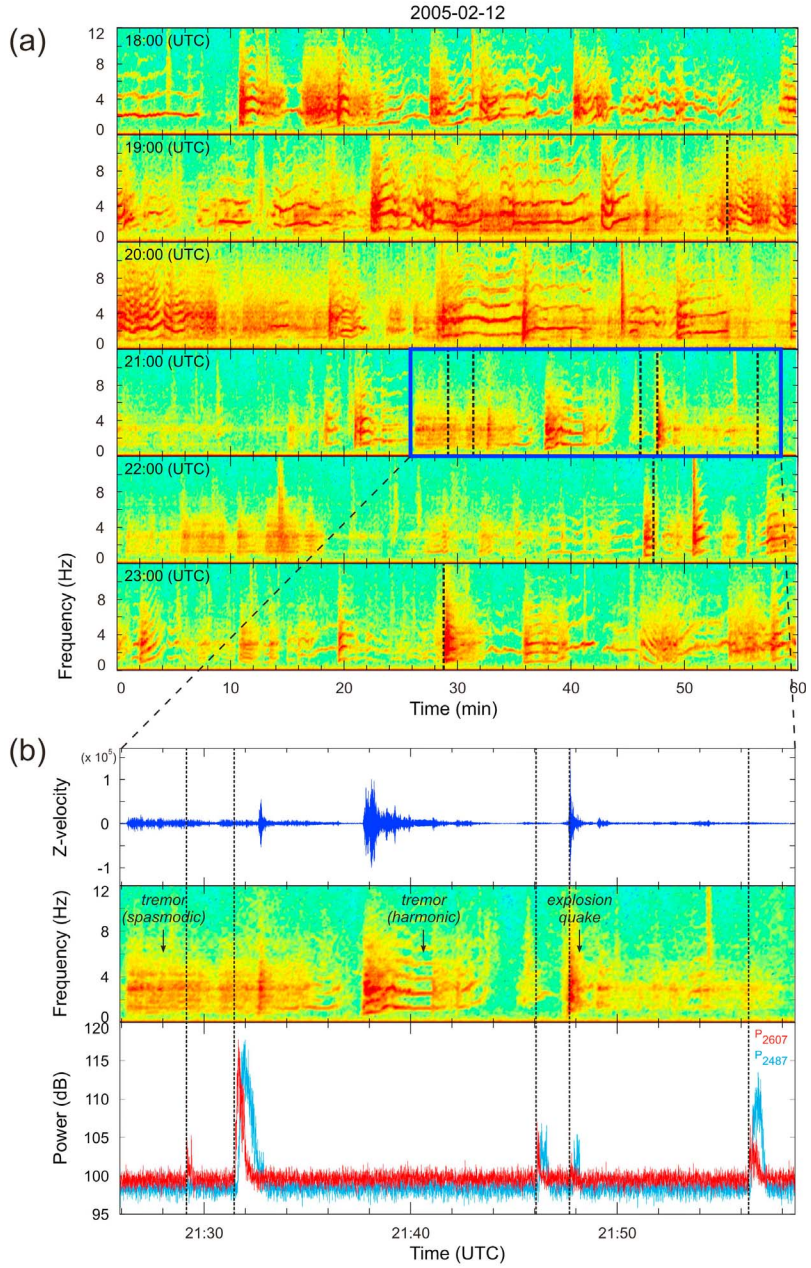

Figure 2. (a) Spectrograms of the seismic signal recorded on February 12, 2005 from 18:00 to 24:00 UTC. Each line corresponds to 1 hour. Vertical dashed lines indicate radar eruptive events. (b) Enlargement of the sequence enclosed by the box in Figure 2a, which presents (from top to bottom) the seismic trace (vertical component), the corresponding Fourier spectrogram, and the power backscattered to the radar in gates G_{2607} (red) and G_{2487} (blue).

[12] Detailed analyses of radar and seismic data were carried out using MATLAB-based software [*Mora et al.*, 2009], we specifically designed for the purpose of this study. This software enables the display of the different data types on a graphical interface and the application of high resolution time-frequency methods [*Lesage*, 2009] to extract the main features from the different geophysical data sets collected. During the 11-day-long field campaign, a total of 132 eruptive events were recorded by the radar, from which we defined a subset of 68 events comprising medium- and large-amplitude radar events, and/or the events having a good seismo-radar temporal correlation.

4. Results

[13] We herein consider the correlation between radar and seismic records on two distinct time-scales: (1) over the time scale of seconds to minutes, to analyze the coeval seismic and radar signals during individual pyroclastic emissions, and (2) at the time scale of several hours, to understand how

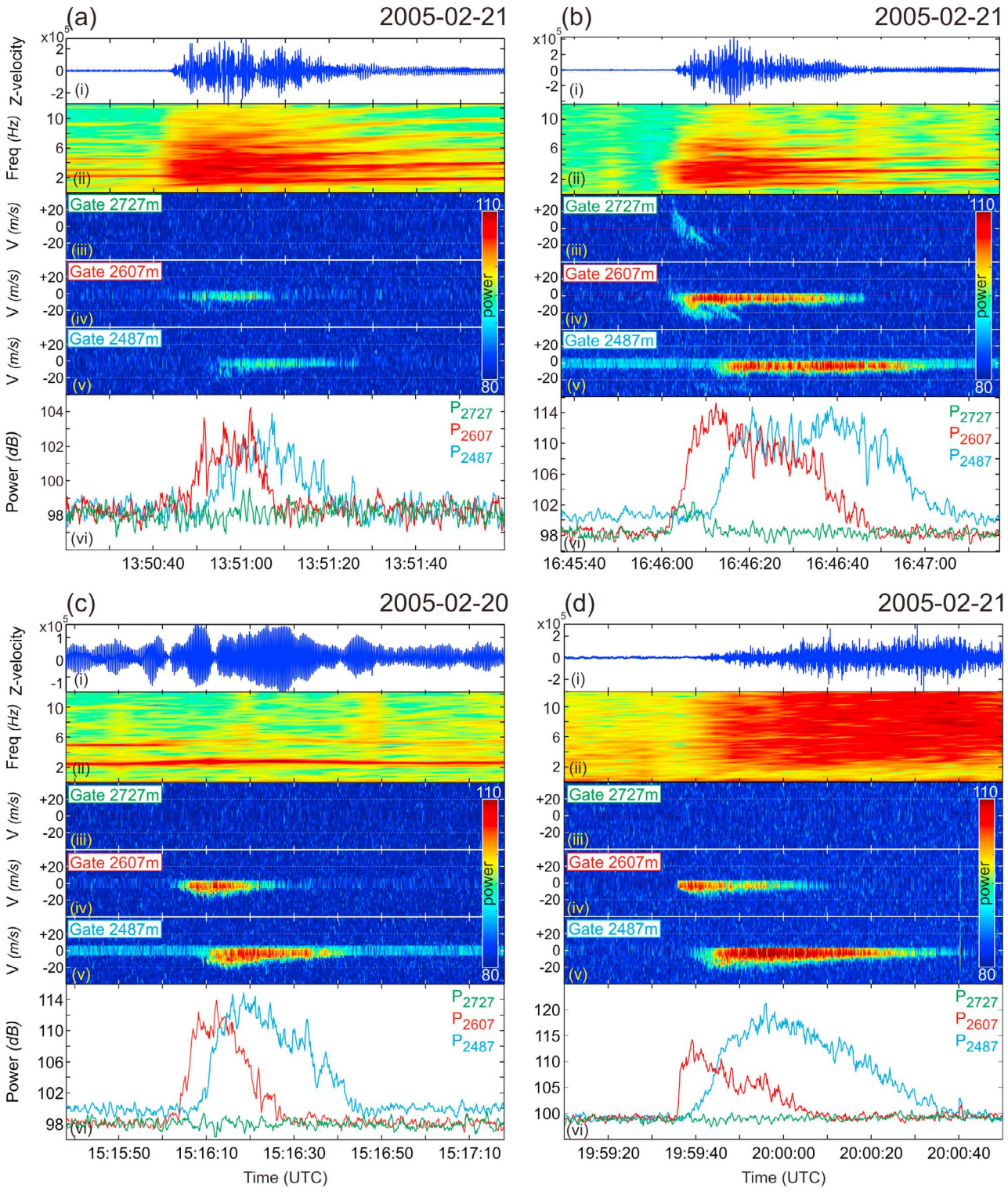

Figure 3. Four representative seismic events and the associated radar signal: (a and b) explosion quakes, (c) harmonic tremor, and (d) no seismic signal at emission onset, post-onset, high-frequency signal only. Figures 3a–3d display the seismic record (plot i); the seismic spectrogram (plot ii); the Doppler radargrams (time-velocity distribution of backscattered radar signal) in gates G_{2727} (plot iii), G_{2607} (plot iv), and G_{2487} (plot v); and the corresponding time series of backscattered power in gates G_{2727} (green), G_{2607} (red), and G_{2487} (blue) (plot vi).

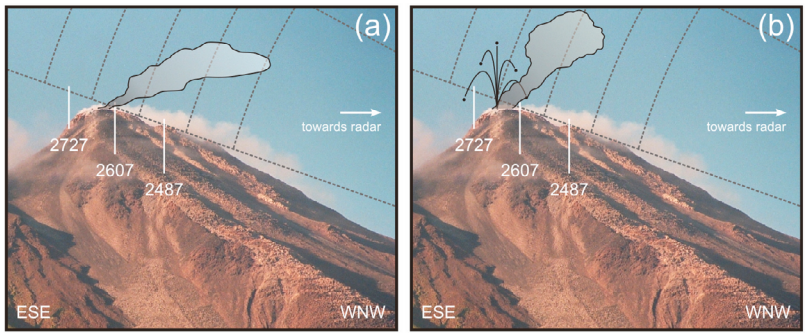

Figure 4. Schematic illustration of pyroclastic emission dynamics, interpreted in terms of spatial motion in the radar range gates. (a) Weakly loaded ash plume drifts in trade winds toward the radar, resulting in Doppler radargrams which exhibit low negative velocities and low backscattered power (e.g., Figure 3a, plots iii–v). (b) Strongly loaded ash plume accompanied by ballistic projections. In this case (e.g., Figure 3b), the resulting radargrams contain an additional signal to the plume signature described previously; the ballistics causing diagonal streaks which exhibit high positive velocities (mostly in gate 2727 m) that progressively shift toward negative velocities.

subsurface and surface activity may interact on longer time scales.

4.1. Short-Term Correlation Between Seismic and Radar Observations

[14] Spectrograms were computed from the seismic data, and radar signals recorded during emissions were traced over it to visualize how surface and sub-surface activity were related on short time scales (Figure 2). Figure 2a shows spectrograms from six consecutive hours of seismic data recorded on the 12 February 2005, with eruptive events detected by the radar being indicated by vertical dashed lines. Figure 2a illustrates the variety of seismic activity discussed in section 2, with sequences of both harmonic and spasmodic tremor, multiple frequency systems that glide independently, numerous explosion quakes, and periods of quiescence all being apparent. Surprisingly, the surface tephra emissions are poorly correlated with this seismic activity. Indeed, tephra emissions detected by the radar are not always associated with distinct seismic events, and emissions can be found associated with explosion quakes (e.g., 23:28:48 UTC), in the middle of tremor sequences (e.g., 21:31:29 UTC), and during periods of very weak seismic activity (e.g., 21:56:23 UTC). This observation applies throughout the entire record in which, of the 68 radar events subset, ~44% of the signals are associated with explosion quakes, ~43% occur during episodes of tremor, and ~13% occur during periods when only background seismic noise is recorded. Figure 2b shows a magnification of the sequence identified by the box in Figure 2a, and highlights that the strongest ash emissions (i.e., the events giving the highest backscattered power, such as that occurring at 21:31:29 UTC) do not occur when they are most expected (i.e., during high amplitude explosion quakes, at 21:37:30 UTC, for example). Hence, it seems that there is no simple relationship between tephra emission and coeval seismic events. Pyroclast emissions do not have a unique repetitive seismic signature and, more importantly, emissions cannot always be identified by the seismic signals alone, even for emissions with high mass loadings.

[15] The radar signals and associated seismic records show a large variability in their respective characteristics. Radar signals show variable backscattered power (varying by more than 30 dB), particle velocities, and Doppler signatures (i.e., time-velocity distribution of the power), which respectively reflect the diversity of the emissions' mass loading, impulsivity and dynamics. Figures 3a–3d display, for several eruptive events, the seismic trace (plot i); its spectrogram (plot ii); (iii-v) the Doppler radargrams (time-velocity distribution of backscattered power) for gates G_{2727} (plot iii), G_{2607} (plot iv), and G_{2487} (plot v); and the radar backscattered power time series for the same gates (plot vi). Figures 3a and 3b are explosion quakes with similar seismic amplitudes, durations and spectral contents. However, the corresponding radar signals are quite different in terms of both backscattered power and radial velocity. While the event given in Figure 3a has a maximum backscattered power that is +7 dB above the noise level and has no positive velocities, the event of Figure 3b has a higher backscattered power (+17 dB), and radial velocities that exceed 20 m/s. Moreover, the radargrams exhibit distinctive Doppler signatures. Figure 3b shows distinctive diagonal streaks during the first few tens of seconds following the eruptive event onset, which is not the case for the event in Figure 3a. These streaks are short-lived (~10 s), are spread across a large velocity range (reaching more than +20 m/s and −20 m/s in gates G_{2727} and G_{2607}, respectively), and seem to superimpose a longer–lived signal (tens of seconds) with low negative radial velocities (less than −10 m/s). *Valade and Donnadieu* [2011] have modeled these short-lived diagonal streaks and show that they result from ballistic blocks crossing the range gates. The longer-lived signal (observed in Figures 3a–3d) instead results from the slow transit of the ash plume through the beam. Hence, although the two events in Figures 3a and 3b have similar seismic signals, the differences in the radar signals reveal two emissions with very different properties, in terms of mass loading, duration, impulsivity and eruptive dynamics. An interpretative sketch of the dynamics of these two events in terms of spatial motion within the range gates, is given in Figure 4. In the case of the event in Figure 3c, a strong radar signal

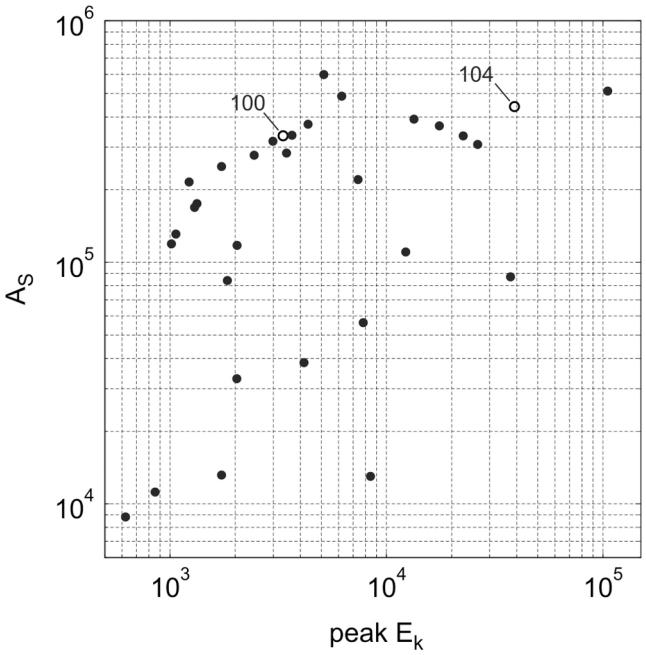

Figure 5. Maximum seismic amplitude A_s (vertical velocity component) versus radar peak amplitude of the kinetic energy proxy E_k, for all the tephra emissions associated with explosion quake events. Values of A_s and E_k are in arbitrary units. Events indexed 100 and 104 refer to the events displayed in Figures 3a and 3b, respectively.

(maximum recorded power ~+17 dB, similar to the event in Figure 3b) occurs without perturbing the harmonic tremor. The event of Figure 3d produces an even stronger signal (with a maximum recorded power of +22 dB). This event is not preceded by any seismic signal, but is followed by a high frequency emergent seismic waveform which begins a few seconds after the radar signal onset. The seismic signal could be interpreted as a rockfall signal, however we doubt that the associated radar signal results from a rockfall-generated cloud. Indeed, the radar signal onset is very impulsive (i.e., sharp P_{2607} increase) and exhibits strong backscattered power (+22 dB), suggesting that a highly concentrated ash plume rapidly entered the beam. In the case of rockfall-originated clouds, we expect much less backscattered power due to both (1) the fine granulometry of the elutriated material and (2) the low particle concentration (compared to ash plumes resulting from an explosive event). Moreover, the radar signal begins before the seismic signal, which is not consistent with a cloud of rockfall-origin. During the recording campaign of 2005, rockfalls were concentrated in a ravine perpendicular to the radar beam axis. This location would increase the time needed for the cloud to rise from its source and drift into the beam. Hence we conclude that this was a highly loaded ash plume, emitted without an associated seismic signal (unlike events in Figures 3a and 3b). All of these observations show that the mass loading (i.e., backscattered power), exit velocities, and dynamics of the tephra emissions at Arenal are highly variable, and do not show apparent correlation with the coeval seismic signal amplitudes or spectral contents.

[16] It is worth noting that both paired and pulsed emissions are commonly observed. Paired eruptions refer to eruptions less than 3 min apart and represent 22% of all the recorded radar events. In most cases, the second event's power amplitude is similar to, or lower than, that of the first (e.g., Figure 2b, 21:46 UTC); only in some rare cases is it higher (e.g., Figure 2b, 21:29 UTC). Pulsed emissions, on the other hand, refer to eruptive events which comprise several pulses, spaced by a few seconds only, as evidenced by the successive streaks in Figure 3b (plot iv). From a seismic point of view, these double-features are rarely recorded, highlighting once again the complex relationship linking the pyroclastic emissions and the coeval seismic signals at Arenal.

[17] Seismic and radar energy proxies were computed for all pyroclastic emissions associated with explosion quake seismic signals. The maximum seismic amplitude (vertical component, A_s) was considered as a suitable proxy for the intensity of the sub-surface process. The use of seismic amplitudes (i.e., velocity trace amplitude) rather than seismic energies (i.e., time-integration of the squared velocity) was preferred because many explosion quakes occurred during background tremor (e.g., Figure 3c), which makes the estimation of the explosion energy problematic. For the radar signal, we computed the kinetic energy, as defined in section 3, for the two gates above the active crater (i.e., $E_{k\ 2607}$ and $E_{k\ 2727}$), and define their sum as the kinetic energy (E_k) of the pyroclastic emissions. Figure 5 displays the maximum seismic amplitude versus the maximum kinetic energy for these events. The data points show a positive trend, which is particularly apparent in the cluster of points in the upper left corner of the plot (i.e., those having A_s between 10^5 and 10^6, and E_k between 10^3 and 10^4, in arbitrary units). The events of this cluster share an emergent onset, a relatively weak power amplitude (<12 dB), and low radial velocities (<16 m/s). Despite this weak positive trend, Figure 5 shows a wide scatter of data points indicating that the ratio between subsurface seismic energy and surface kinetic energy is highly variable. For example, although the events in Figure 3a and 3b (respectively indexed 100 and 104 in Figure 5) have similar seismic amplitudes, they have considerably different kinetic energy values. Whatever the type of energy proxies used for the seismic and radar signals (signal amplitudes, time-integrated energies, various frequency bands, etc.), they all show similarly poor correlation. This suggests poor scaling between the seismic energy and the energy of the subsequent emission. Similar observations were reported by *Johnson et al.* [2005] at Tungurahua. Nevertheless, pyroclastic emissions may be the result of long pressurization processes, which can only be revealed by examining data records on longer time-scales, as reported next.

4.2. Long-Term Correlation Between Seismic and Radar Observations

[18] The time-averaged amplitude of the seismic trace, termed RSAM (Real-time Seismic Amplitude Measurement [*Endo and Murray*, 1991]), has proved capable of revealing long-term cyclic patterns [e.g., *Denlinger and Hoblitt*, 1999]. The cumulative squared amplitude of the seismic trace, or cumulative RSEM (Real-Time Seismic Energy

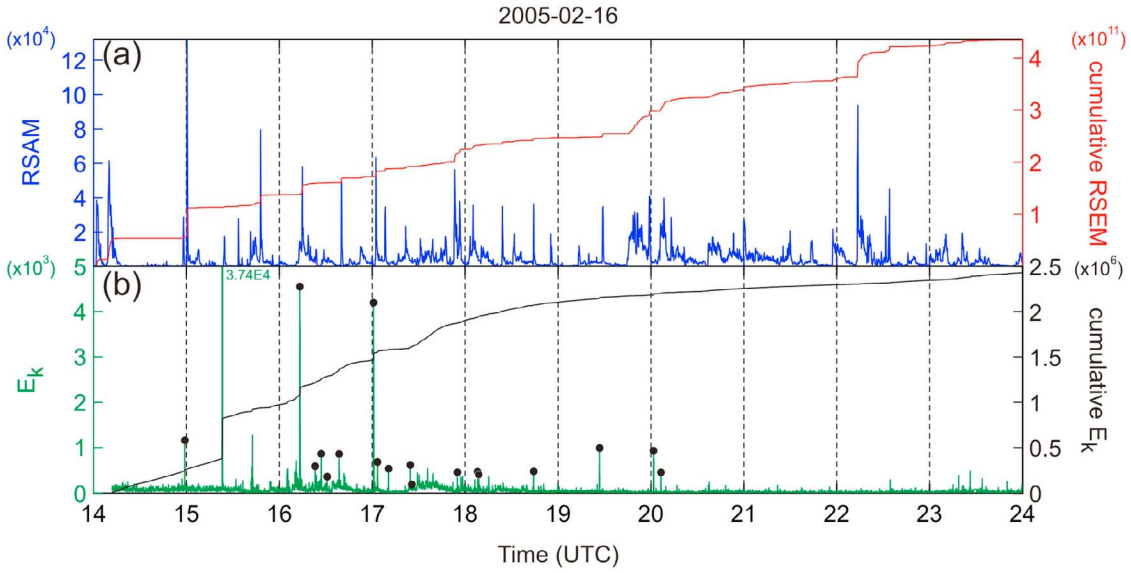

Figure 6. (a) RSAM and cumulative RSEM recorded on the 16 February 2005 and (b) radar kinetic energy (E_k) with its cumulative curve. The kinetic energy curve (E_k) is filtered with a running average, and the recorded eruptive events are indicated by black dots. The peaks which are not topped by black dots are noneruptive peaks (e.g., rain, noise, etc.). For visualization purposes the E_k ordinate axis was clipped at $E_k = 5 \times 10^3$, truncating the major radar event at 15:23 UTC ($E_k = 3.74 \times 10^4$, in arbitrary units).

Measurement [*De la Cruz-Reyna and Reyes-Dávila*, 2001]), enables a better visualization of the seismic energy release rate through time. RSAM, RSEM and E_k time series were thus computed and plotted together to search for relationships between the seismic activity and the tephra emissions on time scales of several hours. Figure 6a and 6b show 10 h of continuous seismic and radar recordings on the 16 February 2005. The RSAM plot displays successive transients with sharp onsets followed by slow decays, which mostly relate to tremor amplitude fluctuations. When an explosion quake triggers a tremor sequence, the RSAM shows a high peak marking the transient onset. The cumulative RSEM curve, on the other hand, shows a gradual increase, punctuated by sudden increments (or steps) when strong explosion quakes are recorded. Similarly, the E_k curve shows successive peaks (or steps in the cumulative E_k curve), indicating the occurrence of pyroclastic emissions with strong kinetic energies. Comparison of Figures 6a and 6b shows poor correlation between the seismic and radar signals: neither the fluctuations (i.e., amplitude oscillations in the RSAM and E_k curves), nor the sudden energy releases (i.e., the steps in the RSEM and E_k cumulative curves), show correlation in time or amplitude. This was observed throughout the entire recording period,

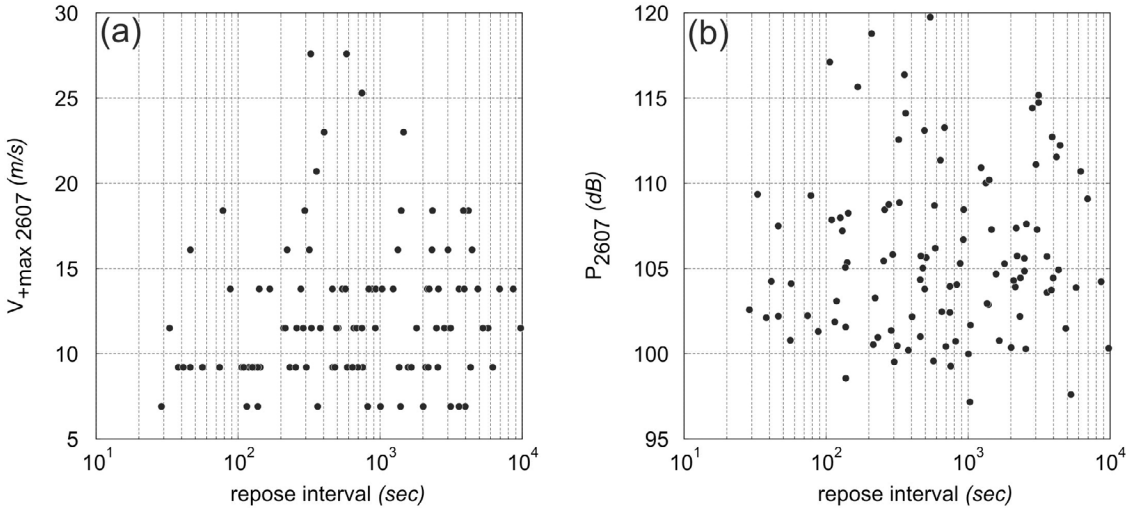

Figure 7. Relationship between the repose interval separating successive tephra emissions and their (a) maximum radial velocities and (b) maximum backscattered power. Values are taken from the main gate G_{2607}.

indicating that there is no simple relationship between the energy of tephra emissions and the energy of seismic vibrations, even on daily time scales.

[19] Classically, exit velocities of volcanic ejecta are thought to be related to overpressures in the volcanic conduit prior to the explosion [*Wilson*, 1980]. If pressure builds-up progressively beneath a cap which obstructs degassing, and if this pressure is released during eruptive events, then the longer the repose intervals between successive eruptions, the longer the period of pressurization and, thus, exit velocities should be higher. Note that this statement holds only if we assume that passive degassing is minor compared to the degassing during an explosion. We consequently investigated whether the measured exit velocities were proportional to the repose interval separating successive emissions. Figure 7a plots the maximum positive radial velocity recorded in gate G_{2607} as a function of repose time, and shows a wide scatter, indicating no correlation between repose time and exit velocity. This suggests that overpressures do not increase steadily during repose intervals, probably because of the fractured nature of the lava cap which allows gas to escape between eruptive events. Figure 7b displays the maximum power recorded in gate G_{2607} as a function of repose time. Again no correlation is observed, which indicates that ejecta mass loadings do not appear to be controlled by the duration of repose.

[20] In summary, analysis of simultaneous seismic and radar recordings show complex, nonrepeatable relationships, on both short and long time scales. Tephra emissions are not systematically associated with a specific type of seismic signal (Figure 2), and show variable properties (i.e., mass loading, exit velocity, dynamics) that do not correlate with seismic amplitude or spectral content (Figure 3). When considering the emissions associated with explosion quakes, poor scaling is found between the kinetic energy of the emission and the amplitude of the seismic signal (Figure 5). Even on daily time scales, we find that the energy of the emissions do not correlate with fluctuations in the seismic amplitude and energy (Figure 6).

5. Existing Models for Arenal-Type Eruptive Activity and Associated Geophysical Signals

[21] Several models have been proposed to account for the style of repeated, mildly explosive eruptive activity and associated geophysical signals at persistently active volcanoes such as Arenal. The physical processes involved in each model depend mainly on the magma viscosity. The bubble-bursting model is widely accepted at volcanoes with low-viscosity magmas. Laboratory experiments [*Jaupart and Vergniolle*, 1988; *Ozerov*, 2010] model the phenomenon as bubbles rising up the conduit to burst intermittently at the surface. This mechanism, however, requires low viscosity magma (10^3 and 10^5 Pa/s [*Ozerov*, 2010]) if the slugs that generate the explosion are to ascend buoyantly through the magma column and burst at the free surface. At Arenal these conditions are not fulfilled: average viscosities of lavas close to the crater range between 10^5 and 10^6 Pa/s [*Cigolini and Borgia*, 1980; *Cigolini et al.*, 1984; *Bertolino et al.*, 2009], and the vent is capped by a degassed, cooled plug of lava [*Cole et al.*, 2005].

[22] The pressure build-up model is often invoked to explain repeated, discrete, short-lived explosions characteristic of the Vulcanian activity. These are attributed to the steady build-up of pressure below a plug obstructing the conduit, which is suddenly released when the plug's resistance threshold is overcome [*Stix et al.*, 1997; *Melnik and Sparks*, 2002; *Yokoo et al.*, 2009]. This sudden failure and decompression causes both brittle failure of the plug and rupture of numerous small gas bubbles trapped in the viscous melt, both of which generate fine ash. At Arenal, petrological observations show that a rigid degassed cap has progressively developed and muzzled the summit vent [*Cole et al.*, 2005]. *Cole et al.* [2005] studied tephra clast morphologies and reported a dominance of blocky textured clasts over fluidal ones, thus arguing for fragmentation of rigid degassed magma with only a minor molten component, typical of Vulcanian-type explosions. The presence of such a degassed body could act as a plug, which blocks the vent and impedes the release of gas.

[23] The idea that such plugs can possess a network of fractures has led several authors to believe that the small pathways represented by the fractures can control the degassing periodicity and, in turn, the associated geophysical signals [*Hellweg*, 2000; *Johnson and Lees*, 2000; *Lesage et al.*, 2006]. The soda-bottle model was proposed by *Hellweg* [2000] as a possible source model for Lascar's harmonic tremor and cyclic degassing behavior. Following *Soltzberg et al.* [1997], *Hellweg* [2000] described how a small opening in a soda bottle may generate cycles of pressure drop beneath the cap, which triggers bubble nucleation and ascent. *Johnson et al.* [1998] and *Johnson and Lees* [2000], on the other hand, proposed a mechanism analogous to a pressure-cooker for Karymsky, in which the plug atop the conduit acts as a valve. In this case, harmonic tremor is the result of rhythmic gas release through the valve, producing source pulses that are sufficiently regular to generate harmonics. More recently, *Lesage et al.* [2006] proposed a process similar to that of a clarinet to explain Arenal's tremor. This model is close to the pressure-cooker idea of *Johnson and Lees* [2000] in the sense that both suggest that gas periodically escapes through fractures in a solid plug. The clarinet model, however, includes a stabilization mechanism for the pressure pulses. As fractures open intermittently, pressure waves are emitted in the conduit, which allow a standing pressure wave to be maintained. This, in turn, controls the pressure state below the plug and consequently the fracture oscillations. This feedback is thought to be an efficient way to produce pressure transients with a stable repeating period, responsible for the harmonic tremor [*Rust et al.*, 2008]. Lack of period stability, however (if rubble chokes the fractures for instance), would result in spasmodic tremor. If the repeat frequency slowly varies with time, the spectral peaks will also vary, and appear as frequency gliding episodes. Nevertheless, if the clarinet-model is an adequate model for the source of tremor at Arenal, it does not explain the source mechanisms of the explosion quakes.

[24] Stick-slip movement of the uppermost part of the conduit has been proposed as a possible conduit model for several volcanoes with high-viscosity magmas, such as Soufriere Hills (Montserrat) and Santiaguito (Guatemala). *Denlinger and Hoblitt* [1999] first suggested that the cyclic

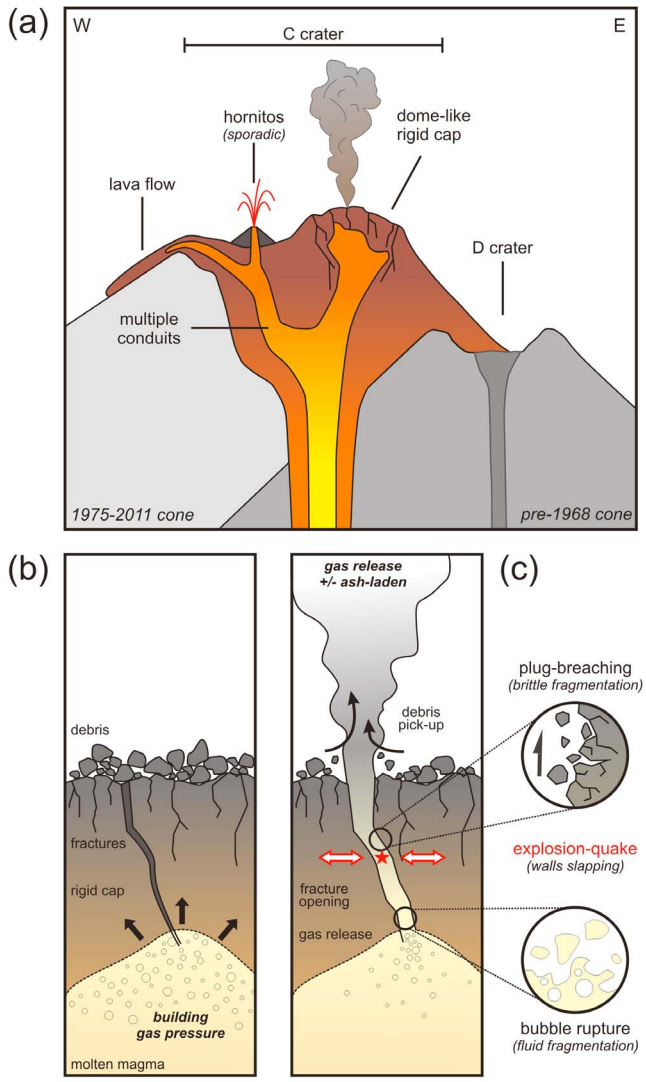

Figure 8. (a) Cross section of Arenal's shallow structure and (b and c) conceptual model of the mechanism of gas and ash emissions at Arenal. In Figure 8b, pressure builds up under a viscous degassed cap crosscut by fractures. When the fracture strength is overcome, the gas is suddenly released (Figure 8c): Fracture walls slap together, triggering high-frequency seismic vibrations characteristic of the explosion quake signals. The turbulent gas may in turn pull out varying quantities of pyroclast, which can be detected by the radar if enough is expelled. The expelled tephra may result from syn-eruptive fragmentation (brittle or fluid fragmentation), or may result from remobilization of loose fragmented material residing atop the cap, or within its permeable fractures.

eruptive behavior at Soufriere Hills might be controlled by boundary conditions along the upper part of the conduit, where stick–slip boundary conditions would generate periodic conduit flow. Field evidence (at Santiaguito, Guatemala [*Bluth and Rose*, 2004]) and numerical modeling [*Gonnermann and Manga*, 2003] have suggested that nonexplosive fragmentation of magma near conduit walls (where strong shear-stress is expected) could generate fine ash during slip events and result in repetitive ash plumes during stick-slip cycles, a hypothesis which was supported by a ring-shaped vent structure and ash emission patterns observed at Santiaguito [*Bluth and Rose*, 2004; *Sahetapy-Engel et al.*, 2008; *Sahetapy-Engel and Harris*, 2009]. Santiaguito, in particular, is very similar to Arenal in terms of eruptive style, intensity and frequency. Both volcanoes show repeated low energy explosions (several per day), sending ash-plumes up to ≤1–4 km, occasionally generating small pyroclastic flows, with a viscous lava cap plugging a conduit from which lava flows continuously extrude. However, at Arenal the characteristic vent structure and emission pattern reported for Santiaguito have not been observed. Furthermore, the constantly evolving crater morphology and the multiplicity of the feeding conduits at Arenal suggest that the persistence of such annular stick-slip zones is unlikely. However, we cannot exclude the possibility that shear-induced fragmentation may occur locally, along limited surfaces of conduit walls.

[25] In summary, pressure build-up under a viscous degassed cap, which is crosscut by fractures, seems the most adequate model to characterize the eruptive periodicity and associated tremor signal at Arenal. Nevertheless, the mechanism explaining the explosion quakes, and the way these are related to the pyroclastic emissions remains unclear. Hence for now, no model can fully account for the complexity of Arenal's activity.

6. Discussion

[26] The joint observation of gas and ash emissions by seismic and Doppler radar measurements reveals complex behavior at Arenal. The seismicity displays a great diversity of event types, which include tremor (both spasmodic and harmonic, with complex frequency gliding episodes) and explosion quakes (of variable amplitude, sometimes followed by a harmonic tremor coda). The radar measurements also reveal great variability in the mass loading and exit velocities of pyroclastic emissions. However, there is poor correlation with the seismicity, and while some mild explosion quakes observed in the seismic records are not accompanied by ash emission, some radar events are not coeval with a seismic signal. Sometimes ash emissions occur during harmonic tremor, or are associated with high frequency (5–35 Hz) seismic events. When pyroclastic emissions and explosion quakes are concomitant, low correlation is obtained between the kinetic energy of the emission and the seismic amplitude. Moreover, no clear relationship can be observed between repose time and exit velocity of solid particles or mass loading of the plume. All of these observations point to a mechanism of gas and ash emission that is highly variable and probably very sensitive to small perturbations in the system.

6.1. Conceptual Model

[27] To explain these observations, we propose the conceptual model of Figure 8. According to this model, fractures in the solid plug control degassing, which in turn controls the seismic signal. If gas release is frequent and intermittent, repetitive pressure pulses will generate low-frequency tremor signal, whereas if gas release is sudden, flow induced vibrations will generate high-frequency explosion quake signals. We hereafter define an explosion as

the release of a given volume of gas, more or less laden with solid particles, through a fracture in the solid plug which becomes suddenly opened to release the gas pressure. We suggest that the high-frequency components of the associated seismic signal (i.e., the explosion quake) result mainly from the interaction between the pressurized turbulent flow of gas and the rough channel walls. Two mechanisms of flow-induced vibration can be considered, whereby hydrodynamic flow instabilities and oscillations occur at the channel walls [*Rust et al.*, 2008]. In the first case, the fluid flow in a thin channel generates roll waves (i.e., waves of channel thickness variation) in the elastic walls when the flow speed is higher than

$$U_{crit\ roll} \approx \beta \sqrt{\frac{\rho_s}{\rho_f}} \frac{H}{L}, \tag{2}$$

where β is the shear wave velocity of the walls, ρ_s/ρ_f the rock to fluid density ratio, and H and L are the thickness and length of the channel, respectively. If we consider typical rock property values of β = 1 km/s and ρ_s = 2000 kg/m^3, with a gas density (ρ_f) of 300 kg/m^3 (H_20 at 500°C and 50 MPa) and, because the fracture is closed at the beginning of the explosion, $H \sim 0$ so that the ratio H/L is small ($\sim 10^{-5}$ to 10^{-3}) during the opening of the fracture, the threshold condition for roll waves to be generated is easily met. However, the channel must be long enough for these instabilities to develop.

[28] The second mechanism is the excitation of normal modes of the conduit walls. Instability occurs when the flow velocity is higher than

$$U_{crit\ wall} \approx fL, \tag{3}$$

where f is the modal frequency and L the characteristic length, or width, of the channel. *Rust et al.* [2008] carried out laboratory experiments of gas flow between an elastic membrane and a rigid plate to show that the amplitude of oscillations increases with increased flow speed (when $U > U_{crit\ wall}$). In another experiment where air was forced to flow through a slit in a block of gelatine, they showed that at very high flow velocities, the channel walls slap together producing large and nonperiodic high-frequency elastic waves. We propose that this process could be considered as an analog for the explosion quakes at Arenal (Figure 8c). In the case of strong explosions, the fracture and part of the plug are destroyed and the conduit remains partly open. However, for most explosions in 2005 at Arenal, the gas volume and pressure associated with each explosion was small, so that the fractures were not, or only slightly, damaged by the gas flow and so that they could close again after the event.

[29] The turbulent gas flow may entrain varying quantities of pyroclasts, and depending on its mass loading, may be recorded by the radar. Explosions expelling only gas will not be detected by the radar (and thus will result in explosion quakes without a coeval radar signal, e.g., Figure 2b, 21:38 UTC). On the other hand, those expelling ash-laden gas flow will produce a radar echo (i.e., explosion quakes with coeval radar signal, Figure 2a, 23:29 UTC). Depending on the fracture strength and the underlying gas pressure, the pyroclasts will not necessarily be expelled all at once, and may result in paired eruptions (i.e., eruptions that are ≤3 min apart, Figure 2b at 21:29 and 21:46 UTC) or pulsed emissions (i.e., pulses ≤10 s apart, Figure 3b, plot iv). In most cases, the second event releases less tephra than the first, ejecting the remaining unevacuated material. The short time lapse separating each eruptive event (minutes to tens of minutes, Figure 2) suggests a high capacity for the system to regenerate overpressure over a very short time scale.

[30] When the gas-flow is intermittent through the fractures of the solid plug, it is believed to act as the source mechanism of tremor [*Lesage et al.*, 2006; *Rust et al.*, 2008]. It results from the periodic opening and closure of the fracture triggered by pressure oscillations associated with standing waves in the conduit. The periodic pulses generate evenly spaced spectral peaks by a Dirac comb effect. This is consistent with the results of moment tensor inversion of tremor waveforms which have been interpreted as the opening and closure of a shallow crack [*Davi et al.*, 2012]. It is also consistent with the repeated large amplitude oscillations (1–2 s) observed in many radar signals associated with ash emissions that suggest staccato pressure release [*Donnadieu et al.*, 2008], and with recent observations of correlation between SO_2 emission rate and tremor amplitude at Fuego volcano [*Nadeau et al.*, 2011]. Furthermore, it explains the frequently observed tremor-like coda of explosions, which occur if the fracture can still act as a valve and if the residual pressure below the plug is high enough after the explosion, or if another crack is opened by the main event. During this kind of post-explosive tremor, the pressure is progressively released by the gas escaping through the fracture. Therefore, the gas flow rate in the upper part of the conduit decreases, the average wave velocity in the resonating conduit increases and thus the fundamental frequency and overtones of the tremor also increases. Simultaneously, the pressure reduction induces an increase of gas exsolution of the magma that tends to counterbalance the gas loss. However, the characteristic time of exsolution and gas transfer inside the conduit is larger than that of the gas loss through the fracture. As a consequence, the dominant effect is a pressure release during the first minutes after mild explosions. This process gives an explanation to the positive frequency gliding observed in the post-explosion tremor (e.g., Figure 2a, 23:02 UTC). On the other hand, during tremors that are not associated with explosion, either constant frequency content, or positive/negative frequency gliding can be obtained according to the balance between gas escape through the plug and gas input in the resonating conduit from exsolution and transfer.

6.2. Model Sensitivity to Evolving Summit Conditions

[31] All the mechanisms considered in the model described above are quite sensitive to small changes of the state of the conduit and plug. In open-system volcanoes such as Arenal, shallow system conditions may evolve rapidly, causing high temporal variability in both the seismic and radar waveforms associated with explosions. In particular, the presence of a solidified cap, its rheology, heterogeneous fracturing, thickness, debris residing above it, and consequently its permeability to gas, may evolve over time scales ranging from days to seconds (e.g., disruption following an explosion). Variable degrees of "gas-tightness" cause variable gas output through the plug fractures, and thus result in complex frequency gliding episodes in the tremor signal (Figure 2). Temporal

variations in fracture strength cause differential mechanical responses to pressure increases from one event to another. Consequently, gas and ash may be expelled from one or several fractures (or vents) simultaneously or at slightly delayed intervals, and the eruption focus may change from one event to another. In this context, the partitioning of the total eruptive energy (i.e., its distribution among the various types of energy: kinetic and seismic [see *Gerst*, 2010]), is likely to vary significantly, and will thus act as a contributing factor to the lack of seismo-radar correlation. The variation in explosion depth, in particular, is likely to have a major impact as it strongly controls the coupling efficiency of the elastic energy radiated into the ground and atmosphere [*Johnson and Aster*, 2005]. Deep explosions (i.e., ~200 m [*Davi et al.*, 2010]) may produce strong seismic signals and low radar signals (exiting of the fragmented material is impeded), and vice versa for shallow explosions. Eventually, due to the distance between the vent and the seismometers, very shallow explosions might not be recorded seismically if they are not strong enough. This may provide an explanation to the occurrence of eruptions unrecorded by seismometers [*Williams-Jones et al.*, 2001], and to radar events which show high exit velocities with no coeval seismic counterpart.

[32] Furthermore, explosions may fragment variable quantities of magma, either molten (i.e., fluidal fragmentation of juvenile magma) or solid (i.e., breaching of the solid plug) (Figure 8c), as attested by tephra clast analysis [*Cole et al.*, 2005]. In turn, the turbulent gas flow may entrain varying quantities of pyroclasts from the plug fracture system, which may be unrecorded by the radar if the ash load is too low. Moreover, magma fragmentation and tephra emissions may not necessarily be synchronous with explosions-quake signals. Indeed, magma fragmentation may result from viscous shear near the conduit walls [*Gonnermann and Manga*, 2003], and loose particles may remain in the permeable fractured regions to be entrained in ensuing events [*Sahetapy-Engel and Harris*, 2009]. Ash emissions can thus result from remobilization of loose, previously fragmented material residing atop the lava cap and/or in the fractured region of conduit walls, remobilized during degassing events (e.g., tremor episodes, Figure 3c).

6.3. Perspectives

[33] Further geophysical studies are needed to constrain the conceptual model proposed here. Acoustic measurements were carried out during this recording campaign, but unfortunately the data were extremely noisy and thus unusable. Nevertheless, acoustic records are likely to hold crucial information on the mechanical processes operating in both the magmatic conduit and the magma-air interface [e.g., *Hagerty et al.*, 2000]. Thus further seismo-acoustic measurements, coupled with coincident Doppler mreasurements, would greatly increase our ability to constrain a shallow system model. Because the mechanism of the eruptions is thought to be closely related to degassing processes, coincident gas flux measurements would also be helpful. In particular, SO_2 fluxes measured by UV cameras have shown to decrease prior to ash-bearing eruptions at Sakurajima [*Kazahaya et al.*, 2010], which suggests that sealing processes were operating between each eruption. Coupling gas flux and radar measurements is thus likely to be very promising. These additional geophysical measurements, if performed continuously over a long period, should allow us to better analyze the variability of the geophysical signals over longer time scales. Such studies may help to further constrain the complex processes, patterns and feedbacks operating in the shallow system of Arenal, and to better understand the mechanism and evolution of its persistent activity.

7. Conclusion

[34] Joint observation of tephra emissions and subsurface processes was carried out at Arenal using broadband seismometers and a ground-based Doppler radar to quantify surface tephra emissions. Cross-correlation of both signals shows complex, nonrepeatable relationships. Indeed, tephra emissions are not systematically associated to a unique type of seismic event, and seem to occur with no clear correlation with the tremor amplitude fluctuation, the seismic energy release rate, or the repose time between successive emissions. Moreover poor correlations are found between the features of both signals (e.g., kinetic energies, backscattered powers, exit velocities of radar signals, versus seismic amplitude, frequency content). We propose a conceptual model that accounts for the generation of the tremor, the explosion quakes, and their relationship with tephra emissions. We suggest that fractures through a solid cap tapping the conduit control degassing of the shallow system, which in turn control the seismic waveforms and tephra emissions. If the gas release is intermittent, it will produce repetitive pressure pulses and thus generate low-frequency tremor signal. On the contrary if gas is suddenly released after the fracture's strength has been overcome by the underlying pressure, flow induced vibrations will generate high-frequency, explosion quake signals. Depending on the amount of fragmented material carried by the gas, the degassing event will either be accompanied by a radar signal (i.e., ash-laden gas output), or not (i.e., ash-free gas output). The variable shallow system conditions (plug thickness, rheology, fracturing, permeability) are likely to be reset on short timescales, and thus result in nonrepetitive conditions that may account for the variability of the gas and ash emission mechanisms (and resulting seismic and radar signals).

[35] **Acknowledgments.** The 2005 radar and seismic campaign was funded through the INSU-CNRS ACI program and the BQR B2005–09 project of Université de Savoie. Financial support from projects 113-A5-503 and 830-A7-511 from University of Costa Rica, Ministry of Science and Technology (MICIT) and National Council for Scientific and Technological Research (CONICIT) and European Commission 6th Framework Project VOLUME (Contract N° 018471) are acknowledged. Acknowledgments are also due to Claude Hervier for technical assistance, Harold Clenet and Laure Pouchol for help in data processing, and Mathieu Gouhier for fruitful discussions on the topic. The Escuela de Geologia and the Instituto Costarricense de Electricidad provided very helpful logistic support, and particular thanks are due to Luis-Fernando Brenes for his great help in the field. We also thank the staff of the Parque Nacional Volcán Arenal for facilitating fieldwork. M. Mora benefited from the visiting researcher program of OPGC. Reviews of the manuscript by Mathias Hort, Micol Todesco, and Geoff Wadge, as well as editorial handling by Tom Parsons, are warmly acknowledged.

References

Barquero, R., G. Alvarado, and T. Matumoto (1992), Arenal volcano (Costa Rica) premonitory seismicity, in *Volcanic Seismology*, edited by P. Gasparini, R. Scarpa, and K. Aki, pp. 84–96, Springer, Berlin.

Benoit, J. P., and S. R. McNutt (1997), New constraints on source processes of volcanic tremor at Arenal volcano, Costa Rica, using broadband seismic data, *Geophys. Res. Lett.*, *24*(4), 449–452, doi:10.1029/97GL00179.

Bertolino, S., C. Cigolini, and G. E. Alvarado (2009), Viscosity and explosive volcanism: The case of Arenal volcano (Costa Rica), *Eos Trans. AGU*, *90*(52), Fall Meet. Suppl., Abstract V11B-1943.

Bluth, G. J. S., and W. I. Rose (2004), Observations of eruptive activity at Santiaguito volcano, Guatemala, *J. Volcanol. Geotherm. Res.*, *136*(3–4), 297–302, doi:10.1016/j.jvolgeores.2004.06.001.

Chouet, B. A. (1996), Long-period volcano seismicity: Its source and use in eruption forecasting, *Nature*, *380*(6572), 309–316, doi:10.1038/380309a0.

Cigolini, C., and A. Borgia (1980), Consideraciones sobre la viscosidad y la estructura de las coladas: Volcán Arenal, Costa Rica, *Rev. Geogr. Am. Central*, *1*(11–12) 131–140.

Cigolini, C., A. Borgia, and L. Casertano (1984), Intra-crater activity, aa-block lava, viscosity and flow dynamics: Arenal volcano, Costa Rica, *J. Volcanol. Geotherm. Res.*, *20*(1–2), 155–176, doi:10.1016/0377-0273(84)90072-6.

Cole, P., E. Fernandez, E. Duarte, and A. Duncan (2005), Explosive activity and generation mechanisms of pyroclastic flows at Arenal volcano, Costa Rica between 1987 and 2001, *Bull. Volcanol.*, *67*(8), 695–716, doi:10.1007/s00445-004-0402-6.

Davi, R., G. O'Brien, I. Lokmer, C. Bean, P. Lesage, and M. M. Mora (2010), Moment tensor inversion of explosive long period events recorded on Arenal volcano, Costa Rica, constrained by synthetic tests, *J. Volcanol. Geotherm. Res.*, *194*(4), 189–200, doi:10.1016/j.jvolgeores.2010.05.012.

Davi, R., G. O'Brien, L. De Barros, I. Lokmer, C. Bean, P. Lesage, M. M. Mora, and G. J. Soto (2012), Seismic source mechanisms of tremor events recorded on Arenal volcano, Costa Rica, retrieved by waveform inversion, *J. Volcanol. Geotherm. Res.*, *213–214*, 1–3, doi:10.1016/j.jvolgeores.2011.10.008.

De la Cruz-Reyna, S., and G. Reyes-Dávila (2001), A model to describe precursory material-failure phenomena: Application to short-term forecasting at Colima volcano, Mexico, *Bull. Volcanol.*, *63*, 297–308, doi:10.1007/s004450100152.

Denlinger, R. P., and R. P. Hoblitt (1999), Cyclic eruptive behavior of silicic volcanoes, *Geology*, *27*(5), 459–462, doi:10.1130/0091-7613(1999)027<0459:CEBOSV>2.3.CO;2.

Donnadieu, F., G. Dubosclard, P. Allard, R. Cordesses, C. Hervier, J. Kornprobst, and J. F. Lénat (2003), Sondages des jets volcaniques par radar Doppler: Applications à l'Etna, in *Rapport Quadriennal de Comité National Français de Géodésie et de Géophysique (C.N.F.G.G.), 1999–2002, XXIII^e Assemblée Générale de l'Union Géodésique et Géophysique Internationale*, edited by J.-P. Barriot, pp. 119–124, Acad. des Sci., de Paris, Paris.

Donnadieu, F., G. Dubosclard, R. Cordesses, T. Druitt, C. Hervier, J. Kornprobst, J. F. Lénat, P. Allard, and M. Coltelli (2005), Remotely monitoring volcanic activity with ground-based Doppler radar, *Eos Trans. AGU*, *86*(21), 201, doi:10.1029/2005EO210001.

Donnadieu, F., M. Gouhier, J. Fournet-Fayard, and C. Hervier (2008), Applications of pulsed ground-based Doppler radar to the study and monitoring of volcanoes, in *Proceedings of the Ground-Based Radar Observations for Volcanoes Workshop*, edited by G. Wadge and R. A. Robertson, pp. 6–8, Environ. Syst. Sci. Cent., Reading, U. K.

Donnadieu, F., S. Valade, and S. Moune (2011), Three-dimensional transport speed of wind-drifted ash plumes using ground-based radar, *Geophys. Res. Lett.*, *38*, L18310, doi:10.1029/2011GL049001.

Dubosclard, G., R. Cordesses, P. Allard, C. Hervier, M. Coltelli, and J. Kornprobst (1999), First testing of a volcano Doppler radar (Voldorad) at Mt. Etna, *Geophys. Res. Lett.*, *26*, 3389–3392, doi:10.1029/1999GL008371.

Dubosclard, G., F. Donnadieu, P. Allard, R. Cordesses, C. Hervier, M. Coltelli, M. Privitera, and J. Kornprobst (2004), Doppler radar sounding of volcanic eruption dynamics at Mount Etna, *Bull. Volcanol.*, *66*, 443–456, doi:10.1007/s00445-003-0324-8.

Endo, E. T., and T. Murray (1991), Real-time Seismic Amplitude Measurement (RSAM): A volcano monitoring and prediction tool, *Bull. Volcanol.*, *53*, 533–545, doi:10.1007/BF00298154.

Garcés, M. A., M. T. Hagerty, and S. Y. Schwartz (1998), Magma acoustics and time-varying melt properties at Arenal volcano, Costa Rica, *Geophys. Res. Lett.*, *25*(13), 2293–2296, doi:10.1029/98GL01511.

Gerst, A. (2010), The first second of a Strombolian volcanic eruption, Ph.D. thesis, Hamburg Univ., Hamburg, Germany.

Gonnermann, H. M., and M. Manga (2003), Explosive volcanism may not be an inevitable consequence of magma fragmentation, *Nature*, *426*(6965), 432–435, doi:10.1038/nature02138.

Gouhier, M., and F. Donnadieu (2008), Mass estimations of ejecta from Strombolian explosions by inversion of Doppler radar measurements, *J. Geophys. Res.*, *113*, B10202, doi:10.1029/2007JB005383.

Gouhier, M., and F. Donnadieu (2010), The geometry of Strombolian explosions: Insights from Doppler radar measurements, *Geophys. J. Int.*, *183*, 1376–1391, doi:10.1111/j.1365-246X.2010.04829.x.

Hagerty, M. T., S. Y. Schwartz, M. A. Garcés, and M. Protti (2000), Analysis of seismic and acoustic observations at Arenal Volcano, Costa Rica, 1995–1997, *J. Volcanol. Geotherm. Res.*, *101*, 27–65, doi:10.1016/S0377-0273(00)00162-1.

Hellweg, M. (2000), Physical models for the source of Lascar's harmonic tremor, *J. Volcanol. Geotherm. Res.*, *101*(1–2), 183–198, doi:10.1016/S0377-0273(00)00163-3.

Jaupart, C., and S. Vergniolle (1988), Laboratory models of Hawaiian and Strombolian eruptions, *Nature*, *331*(6151), 58–60, doi:10.1038/331058a0.

Johnson, J., and R. Aster (2005), Relative partitioning of acoustic and seismic energy during Strombolian eruptions, *J. Volcanol. Geotherm. Res.*, *148*(3–4), 334–354, doi:10.1016/j.jvolgeores.2005.05.002.

Johnson, J. B., and J. M. Lees (2000), Plugs and chugs—Seismic and acoustic observations of degassing explosions at Karymsky, Russia and Sangay, Ecuador, *J. Volcanol. Geotherm. Res.*, *101*(1–2), 67–82, doi:10.1016/S0377-0273(00)00164-5.

Johnson, J. B., J. M. Lees, and E. I. Gordeev (1998), Degassing explosions at Karymsky volcano, Kamchatka, *Geophys. Res. Lett.*, *25*(21), 3999–4002, doi:10.1029/1998GL900102.

Johnson, J. B., M. C. Ruiz, J. M. Lees, and P. Ramon (2005), Poor scaling between elastic energy release and eruption intensity at Tungurahua volcano, Ecuador, *Geophys. Res. Lett.*, *32*, L15304, doi:10.1029/2005GL022847.

Kazahaya, R., T. Mori, and M. Iguchi (2010), The degassing fluctuation concerning sealing process before eruptions at Sakurajima volcano, Japan, Abstract V52C-06 presented at 2010 Fall Meeting, AGU, San Francisco, Calif., 13–17 Dec.

Lesage, P. (2009), Interactive Matlab software for the analysis of seismic volcanic signals, *Comput. Geosci.*, *35*(10), 2137–2144, doi:10.1016/j.cageo.2009.01.010.

Lesage, P., M. M. Mora, G. E. Alvarado, J. Pacheco, and J.-P. Métaxian (2006), Complex behavior and source model of the tremor at Arenal volcano, Costa Rica, *J. Volcanol. Geotherm. Res.*, *157*(1–3), 49–59, doi:10.1016/j.jvolgeores.2006.03.047.

McNutt, S. R. (2002), Volcano seismology and monitoring for eruptions, in *International Handbook of Earthquake and Engineering Seismology*, *Int. Geophys. Ser.*, vol. 81, edited by W. H. K. Lee et al., pp. 383–406, Elsevier, New York.

Melnik, O., and R. S. J. Sparks (2002), Dynamics of magma ascent and lava extrusion at Soufrière Hills Volcano, Montserrat, *Geol. Soc. London, Mem.*, *21*(1), 153–171, doi:10.1144/GSL.MEM.2002.021.01.07.

Minakami, T., S. Utibori, and S. Hiraga (1969), The 1968 eruption of volcano Arenal, Costa Rica, *Bull. Earthquake Res. Inst. Univ. Tokyo*, *47*, 783–802.

Mora, M. (2003), Etude de la structure superficielle et de l'activité sismique du volcan Arenal, Costa Rica, Ph.D. thesis, Lab. de Géophys. Interne et Tectonophys., Univ. de Savoie, Le Bourget du Lac, France.

Mora, M. M., P. Lesage, B. Valette, G. E. Alvarado, C. Leandro, J.-P. Métaxian, and J. Dorel (2006), Shallow velocity structure and seismic site effects at Arenal volcano, Costa Rica, *J. Volcanol. Geotherm. Res.*, *152*(1–2), 121–139, doi:10.1016/j.jvolgeores.2005.09.013.

Mora, M., P. Lesage, F. Donnadieu, S. Valade, A. Schmidt, G. Soto, W. Taylor, and G. Alvarado (2009), Joint seismic, acoustic and Doppler radar observations at Arenal volcano, Costa Rica: Preliminary results, in *VOLUME Project*, edited by C. J. Bean et al., pp. 330–340, VOLUME Proj. Consortium, Dublin.

Mori, J., H. Patia, C. McKee, I. Itikarai, P. Lowenstein, P. De Saint Ours, and B. Talai (1989), Seismicity associated with eruptive activity at Langila volcano, Papua New Guinea, *J. Volcanol. Geotherm. Res.*, *38*, 243–255, doi:10.1016/0377-0273(89)90040-1.

Murillo, S., and P. Ruiz (2004), Datos paramétricos de las coladas de lava del volcán Arenal (Costa Rica) entre 1968 y 2002, *Boletín Obs. Sismol. Vulcanológico Arenal Miravalles*, *15*(27), 25–33.

Nadeau, P. A., J. L. Palma, and G. P. Waite (2011), Linking volcanic tremor, degassing, and eruption dynamics via SO_2 imaging, *Geophys. Res. Lett.*, *38*, L01304, doi:10.1029/2010GL045820.

Neuberg, J. (2000), Characteristics and causes of shallow seismicity in andesite volcanoes, *Philos. Trans. R. Soc. London A*, *358*(1770), 1533–1546, doi:10.1098/rsta.2000.0602.

Ozerov, A. Y. (2010), The mechanism of basaltic explosions: Experimental modeling, *J. Volcanol. Seismol.*, *4*(5), 295–309, doi:10.1134/S0742046310050015.

Rust, A. C., N. J. Balmforth, and S. Mandre (2008), The feasibility of generating low-frequency volcano seismicity by flow through a deformable channel, in *Fluid Motions in Volcanic Conduits: A Source of Seismic*

and Acoustic Signals, edited by S. J. Lane and J. S. Gilbert, *Geol. Soc. Spec. Publ.*, *307*, 45–56, doi:10.1144/SP307.4.

Sahetapy-Engel, S., and A. Harris (2009), Thermal structure and heat loss at the summit crater of an active lava dome, *Bull. Volcanol.*, *71*(1), 15–28, doi:10.1007/s00445-008-0204-3.

Sahetapy-Engel, S. T., A. J. Harris, and E. Marchetti (2008), Thermal, seismic and infrasound observations of persistent explosive activity and conduit dynamics at Santiaguito lava dome, Guatemala, *J. Volcanol. Geotherm. Res.*, *173*(1–2), 1–14, doi:10.1016/j.jvolgeores.2007.11.026.

Soltzberg, L. J., P. G. Bowers, and C. Hofstetter (1997), A computer model for soda bottle oscillations: "The bottelator, *J. Chem. Educ.*, *74*(6), 711–714, doi:10.1021/ed074p711.

Stix, J., R. C. Torres, L. Narváez M, G. P. Cortés J, J. A. Raigosa, D. Gómez M, and R. Castonguay (1997), A model of vulcanian eruptions at Galeras volcano, Colombia, *J. Volcanol. Geotherm. Res.*, *77*(1–4), 285–303, doi:10.1016/S0377-0273(96)00100-X.

Valade, S., and F. Donnadieu (2011), Ballistics and ash plumes discriminated by Doppler radar, *Geophys. Res. Lett.*, *38*, L22301, doi:10.1029/2011GL049415.

Wadge, G., D. Oramas Dorta, and P. Cole (2006), The magma budget of Volcán Arenal, Costa Rica from 1980 to 2004, *J. Volcanol. Geotherm. Res.*, *157*(1–3), 60–74, doi:10.1016/j.jvolgeores.2006.03.037.

Williams-Jones, G., J. Stix, M. Heiligmann, J. Barquero, E. Fernandez, and E. D. Gonzalez (2001), A model of degassing and seismicity at Arenal volcano, Costa Rica, *J. Volcanol. Geotherm. Res.*, *108*(1–4), 121–139, doi:10.1016/S0377-0273(00)00281-X.

Wilson, L. (1980), Relationships between pressure, volatile content and ejecta velocity in three types of volcanic explosion, *J. Volcanol. Geotherm. Res.*, *8*(2–4), 297–313, doi:10.1016/0377-0273(80)90110-9.

Yokoo, A., T. Tameguri, and M. Iguchi (2009), Swelling of a lava plug associated with a Vulcanian eruption at Sakurajima Volcano, Japan, as revealed by infrasound record: Case study of the eruption on January 2, 2007, *Bull. Volcanol.*, *71*, 619–630, doi:10.1007/s00445-008-0247-5.

Zobin, V. M., G. A. Reyes, E. Guevara, and M. Bretón (2009), Scaling relationship for Vulcanian explosions derived from broadband seismic signals, *J. Geophys. Res.*, *114*, B03203, doi:10.1029/2008JB005983.

G. E. Alvarado and M. M. Mora, Escuela Centroamericana de Geología, Universidad de Costa Rica, San José, Costa Rica.

F. Donnadieu, A. Harris, and S. Valade, Clermont Université, Université Blaise Pascal, Observatoire de Physique du Globe de Clermont-Ferrand, Laboratoire Magmas et Volcans, BP 10448, F-63000 Clermont-Ferrand, France. (f.donnadieu@opgc.univ-bpclermont.fr; s.valade@opgc.univ-bpclermont.fr)

P. Lesage, Institut des Sciences de la Terre, Université de Savoie, CNRS, F-73376 Le Bourget-du-Lac, CEDEX, France.